Journal of
Composites Science

MDPI

Article

Nonlocal Free Vibrations of Metallic FGM Beams

Maria A. R. Loja [1,2,*], Katarzyna Rzeszut [3] and Joaquim I. Barbosa [1,2]

[1] CIMOSM, ISEL—Centro de Investigação em Modelação e Optimização de Sistemas Multifuncionais, Instituto Superior de Engenharia de Lisboa, 1959-007 Lisboa, Portugal; joaquim.barbosa@tecnico.ulisboa.pt
[2] IDMEC, IST—Instituto de Engenharia Mecânica, Instituto Superior Técnico, Universidade de Lisboa, 1049-001 Lisboa, Portugal
[3] Faculty of Civil and Environmental Engineering, Poznan University of Technology, Piotrowo 5, 60-965 Poznan, Poland; katarzyna.rzeszut@put.poznan.pl
* Correspondence: amelia.loja@isel.pt

Abstract: This work aims to analyse the free-vibration response of functionally graded, simply supported beams with different gradient directions, taking into account nonlocal effects. To this purpose, the first-order shear deformation theory and the nonlocal elasticity theory of Eringen are used, in order to assess the influence of size dependency effects on the free-vibration responses of those beams. The influence of other factors such as the aspect ratio of the beams and the evolution of the constituents' mixture through the beam thickness and along its length is also considered. In this last case, a mixture distribution is proposed, accounting for the boundary conditions' characteristics. The finite element model is first verified against existing alternative solutions, to assess and illustrate its performance. Based on the conclusions achieved, a set of parametric studies is then developed. The results are discussed considering the material distribution profiles, and conclusions are drawn with respect to their relative performance under the analysed conditions.

Keywords: Eringen' nonlocal theory; first-order shear deformation theory; functionally graded materials; free vibrations; finite element analysis

Citation: Loja, M.A.R.; Rzeszut, K.; Barbosa, J.I. Nonlocal Free Vibrations of Metallic FGM Beams. *J. Compos. Sci.* **2022**, *6*, 125. https://doi.org/10.3390/jcs6050125

Academic Editors: Konda Gokuldoss Prashanth and Francesco Tornabene

Received: 22 March 2022
Accepted: 21 April 2022
Published: 25 April 2022

1. Introduction

With the increasing use of micro- and nanoscale components and systems in a diversity of engineering and science applications, the need for a more complete understanding of their mechanical behaviour arose as an important research area.

In recent years, the understanding and prediction of the mechanical responses of such structures, considering nonlocal approaches, has been addressed by several researchers. Among these published works, one can refer to Reddy [1], where different beam theories were reformulated by the nonlocal differential constitutive relations of Eringen [2,3], obtaining the equations of motion and their variational statements in terms of the generalized displacements. The nonlocal behaviour of beams was illustrated and analysed through analytical solutions for the bending, vibration and buckling. Later, Reddy and Pang [4] presented analytical solutions based on nonlocal theories of the Euler–Bernoulli and Timoshenko beam theories for the analysis of straight beams subject to diverse boundary conditions under bending, buckling and free natural vibrations. The authors concluded that increasing the nonlocal parameter would diminish fundamental frequencies and buckling loads, while in the opposite sense it would increase the static deflections.

Eringen' theory of nonlocal elasticity states that the stress at a reference point in a continuous body depends not only on the strains at that point but also on the strains at all other points of the body. As such, if one considers that those effects may be neglected, one achieves classical theory of elasticity, which can thus be seen as a particular case of the nonlocal one.

Nejad and Hadi [5] studied the static bending of Euler–Bernoulli nanobeams made of bidirectional metal–ceramic functionally graded material considering small-scale effects.

To this purpose, the authors used Eringen's nonlocal elasticity theory. The generalized differential quadrature method was used to solve the governing equations for various boundary conditions so as to analyse the influence of the material length scale parameter and inhomogeneity on the static behaviour of nanobeams. Moreover, considering Euler–Bernoulli beam theory, Ghaffari et al. [6] developed an analytical solution based on the nonlocal elasticity theory to analyse arbitrary loading profiles and boundary conditions. The authors analysed the influence of size, nonhomogeneity and nonuniform loads on the nanobeams' bending, buckling and vibration behaviours.

Lu et al. [7] proposed a size-dependent sinusoidal shear deformation beam model to study nanobeams' free vibration based on the nonlocal strain gradient theory. Navier's method was used to obtain analytical solutions for natural frequencies of simply supported nanobeams. The authors found that frequencies predicted by nonlocal strain gradient theory were higher than those obtained by nonlocal theory and lower than those obtained by strain gradient theory. In other work by the same authors, Lu et al. [8], a unified, size-dependent, higher-order beam model was developed to study the influence of the nonlocal stress and strain gradient on the bending and buckling responses of nanobeams. It was concluded that the Timoshenko beam model predictions and other higher-order models' predictions were almost the same.

More recently, Danesh and Javanbakht [9] studied the free-vibration behaviour of nonlocal nanobeams using nonlocal integral Timoshenko beam theory and two-dimensional nonlocal integral elasticity theory. Different boundary conditions were considered to assess the first three natural frequencies. The authors concluded on the nonlocal parameters' softening effect on the natural frequencies for all the boundary conditions.

According to Koizumi [10], the concept of a functionally graded material was introduced in 1984 by material researchers in the Sendai area, due to the need to develop thermal barrier materials. These new materials revealed not only that they were able to respond to such requirements but also that, due to the continuous variation in their material composition, they provided a continuous variation of material properties that brought additional gains namely by minimizing abrupt stress transitions. In fact, FGMs are known for their relative advantages when compared to traditional laminates, because they can provide smooth property variations from point to point, which did not happen when considering the interface between laminate plies. Additionally, while at each ply level within a composite laminate one usually finds an anisotropic behaviour, an FGM shows isotropic behaviour at each point in spite of their global heterogeneous nature.

In this context, some review papers have been published, such as the one by Zhang et al. [11], which presents an overview of published work comprising the stability, buckling and free-vibration analyses of FGM structures. Based on that review, the authors also suggest further work pathways. Saleh et al. [12] also presented a comprehensive overview of FGM manufacturing methods and a summary of the diversity of applications and the foreseen future trends for research that will be needed for the design and manufacturing of these materials. Rajak et al. [13] also presented an overview of composite materials, their characterization, classification and main advantages linked to physical and mechanical properties based on recent studies.

Linking the nonlocal approach to the analysis of FGM structures, El-Borgi et al. [14] investigated the free- and forced-vibration response of simply supported FGM nanobeams resting on a nonlinear elastic foundation. Eringen's nonlocal elasticity model with material length scales was jointly used with Euler–Bernoulli beam theory with von Kármán geometric nonlinearity. The effects of nonlocal parameter, power-law index, and the parameters of the nonlinear elastic foundation on the nonlinear frequency response were analysed.

Ebrahimi and Barati [15] investigated the combined influence of moisture and temperature on the free vibrations of FGM nanobeams resting on elastic foundations. The authors used different beam theories able to model shear deformation needless of shear correction factor, and they also assumed the material properties to be temperature dependent and varying gradually through thickness. Size-dependent effects were considered by applying

the nonlocal elasticity theory of Eringen. The influence of hygrothermal loadings, elastic foundation, power-law exponent, nonlocal parameter and beams' slenderness ratio on the free vibrations was analysed.

The free-vibration responses of nonlinear symmetric power and sigmoid functionally graded nonlocal nanobeams were studied by Hamed et al. [16]. In this work, the material mixture was assumed to vary across the thickness and symmetric distribution with reference to the mid-plane, e.g., ceramic–metal–ceramic and metal–ceramic–metal configurations were considered. Nonlocal differential Eringen's elasticity was used to include size-dependent effects. The influences of the distributions, the gradient indexes and nonlocal parameter on the natural frequencies were evaluated.

Aria and Friswell [17] considered the first-order shear deformation theory to propose a finite element model to study free vibration and buckling behaviour of through-thickness FGM nanoscale beams. The stretching–bending coupling effect was eliminated by using the neutral axis concept. Buckling loads and natural frequencies were calculated for different nonlocal coefficients, boundary conditions, power-law exponents and aspect ratios.

Pajand and Mokhtari [18] developed a study on the bending, buckling and free vibration of two-directional FGM nanobeams based on Reddy–Bickford beam theory. Material properties were described by an arbitrary power-law form in both the axial and thickness directions. A symmetric, smoothed, particle hydrodynamics meshless method was used to implement the model and assess the effects of gradient indexes, boundary conditions, size scale parameters, aspect and elastic modulus ratios on static and dynamic responses.

A higher-order element based on Timoshenko beam theory and considering a two-node beam element with Hermitian functions of a fifth-degree polynomial was proposed by Katili et al. [19] to perform static and free-vibration analyses of FGM beams. The influence of different boundary conditions and the exponent of the FGM power law were assessed and allowed the conclusion that the coupling of axial bending has a relevant influence.

Uzun and Yayli [20] studied the free vibration of through-thickness FGM nanobeams resting on Winkler–Pasternak elastic foundations, using Euler–Bernoulli beam theory and Eringen's nonlocal elasticity theory. A parametric study was carried out to characterize nonlocality effects. Akgöz and Civalek [21] studied the bending response of nonhomogenous, simply supported microbeams embedded in an elastic medium using the modified strain gradient elasticity theory jointly with different beam theories. The elastic medium was modelled as a Winkler foundation, and the bending problem of the FGM simply supported microbeams was solved using Navier's procedure. Sobhy [22] investigated the bending response, free vibration, mechanical buckling and thermal buckling of FGM nanoplates in a Pasternak foundation. The material mixture was assumed to vary through the thickness. The Eringen's nonlocal elasticity theory was also considered to derive the equations of motion from Hamilton's principle. The author studied the influence of nonhomogeneity, nonlocal parameters, elastic foundation stiffness, plate aspect ratio and side-to-thickness ratio on the nanoplates' response. The size-dependent behaviour of FGM microbars was investigated by Rahaeifard [23] using the modified couple stress theory. The equation of motion and corresponding boundary conditions were derived using Hamilton's principle to study the static and dynamic behaviour of a microbar with fixed–free boundary conditions.

Considering a more specific type of composite material, namely the metal functionally graded materials, where comparatively a minor number of works has been published, Sobczak and Drenchev [24] carried out a review in the area of metal FGMs, on their characterization, properties and production methods, mainly focussing on systematizing manufacturing techniques. Experimental and theoretical methods for the qualitative and quantitative estimation of properties evolution profiles were also considered.

Later, Chen and Liou [25] made a survey study concerning research progress in metal FGMs by additive manufacturing (AM) in which findings in the research and development of major types of AM are discussed. The authors also addressed the technical aspects of metal FGMs' AM and their industrial applications.

Kumar and Chaudhary [26] recently denoted the importance of aluminium composites as the most potential candidate for structural and functional applications, in diverse application fields such as in marine, defence, automotive, aerospace and heat-prone areas. This review article addresses this topic in a comprehensive perspective with regard to mechanical properties, the effect of various reinforcements, various challenges and future research potential in the development of composites. In line with this research potential, Sudherson at al. [27] discussed the positive effect of using cadmium on aluminium alloys to achieve better characteristics for application sectors in which corrosion and wear are more severe. The authors also concluded on the need to develop further studies in the vast area of metal matrix composites.

It is in this context that one presents a study on the free-vibration behaviour of moderately thick and thin metal–metal functionally graded beams ruled by through-thickness and lengthwise material phase mixture. Material phase mixture can have an important effect in a FGM structures' response; therefore, in the analysis of non-thick beam structures, it is likely that a lengthwise mixture distribution can play a significant influence when compared to a through-thickness one. This design variable can also be suited to deal with different beam boundary conditions, thus being the reason for the proposed distribution. These were the aspects that motivated this work, and they have not been addressed as far as the authors' knowledge in other published works.

A nonlocal first-order beam model is developed and implemented, and parametric studies are carried out to characterize nonlocality effects in connection to other beam characteristics. The model is verified against other authors' solutions, showing a very good agreement. It is also verified that the proposed lengthwise distribution is able to confer an improved free-vibration response for the considered beams.

2. Materials and Methods

2.1. Functionally Graded Materials

Given the tailormade characteristics of composite materials, functionally graded materials are also well known for this capability. In this latter type of composite, the constituents' mixture is ruled by mathematical expressions, which can either correspond to the designed composition evolution that one desires the materials to present or correspond to the one that those materials effectively present, as in the works [28,29].

In the present work, one considers the possibility of the materials' mixture to occur both through the beam thickness Equation (1) and along the beam length (Equation (2)). In the first case, we will use the well-known power law [30–34], and in the second case, we propose a symmetrical evolution of the mixture, centred at the beam mid-span considering that we aim to specifically address simply supported beams.

$$V_f = \left(\frac{1}{2} + \frac{z}{h}\right)^{pz} \tag{1}$$

$$V_f = \left| \frac{\left(x - \frac{L}{2}\right)}{\frac{L}{2}} \right|^{px} \tag{2}$$

where V_f represents the volume fraction of a specific phase (to choose); h and L denote the thickness and the length of the beam, respectively; and the exponents pz and px are adjustment parameters that govern the mixtures' rate, as illustrated in Appendix A.

The last distribution is inspired by a previous work in the context of variable stiffness plates' analysis [35].

For each of these volume fractions' distributions, two different FGMs will be considered according to Voigt rule of mixtures, as in Equations (3) and (4).

$$E_{FGM1} = V_f E_{Al} + \left(1 - V_f\right) E_{Cd} \tag{3}$$

$$E_{FGM2} = V_f E_{Cd} + \left(1 - V_f\right) E_{Al} \tag{4}$$

with E_{FGMt} representing the Young's modulus of the FGM (t = 1,2), and E_{Al}, E_{Cd} standing for the Young's modulus of aluminium and cadmium, respectively.

The constituent materials that will be considered in this work are aluminium and cadmium, not only because of their chemical compatibility [26] but also due to the improved wear that cadmium brings to the aluminium [27], hence being relevant to the assessment of the mechanical behaviour of such materials.

The material distributions will then be designated as FGM1-K or FGM2-K depending on whether they are ruled by the rule of mixtures defined in Equations (3) or (4), respectively. The K variable associated to the designation of the material, may assume the character X or Z depending on whether the material mixture evolution occurs along the length (x) or through the thickness (z) direction, respectively; thus, leading to four possible situations: FGM1-X, FGM1-Z, FGM2-X and FGM2-Z.

In the implementation stage, the FGM1-X and FGM2-x distributions were first submitted to a variable change procedure within each finite element calculation, to carry out the corresponding integrations in $[-1..1]$.

The Voigt' rule of mixtures was also considered to estimate the effective Poisson's ratio of the functionally graded materials, although in this last case, this quantity is equal for both material constituents. These dual-phase composites will be considered later in the numerical applications section.

2.2. Constitutive Relations and Equilibrium Equations

2.2.1. Displacement and Strain Fields

The first-order shear deformation' displacement field that describes the beam kinematics in the xz plane, can be written as [36]

$$\begin{array}{c} u(x,z,t) = u^0(x,t) + z\theta_x^0(x,t) \\ w(x,z,t) = w^0(x,t) \end{array} \tag{5}$$

where u^0, w^0 are the mid-plane displacements along the x and z directions, which are in correspondence to the length and thickness directions of the beam (Figure 1).

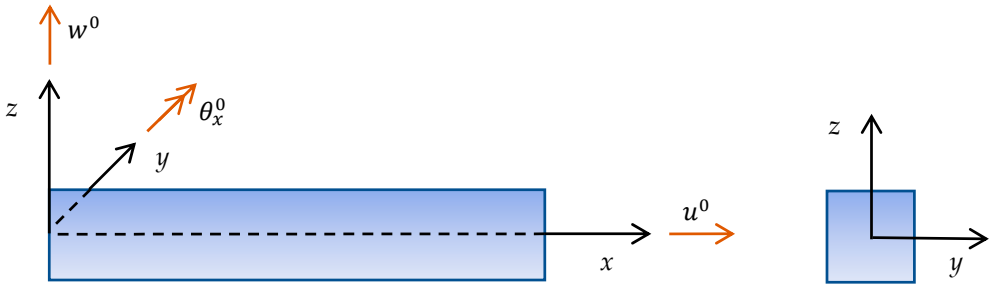

Figure 1. Beam coordinate system and displacement field's degrees of freedom.

θ_x^0 is the rotation of the beam' mid-plane around the y direction. The superscript 0 denotes the association of the degree of freedom to the mid-plane of the beam. The model based on this displacement field will be referred to as FSDT in short.

The corresponding strain displacement is obtained by applying the elasticity kinematical relations for small deformations to the displacement field, as in Equation (6). The axial strain ε_x is described as a linear function of the thickness coordinate, and the transverse shear strain γ_{xz} denotes the known constant profile through the thickness.

$$\begin{array}{c} \varepsilon_x = \frac{\partial u^0}{\partial x} + z\frac{\partial \theta_x^0}{\partial x} \\ \gamma_{xz} = \left(\frac{\partial w^0}{\partial x} + \theta_x^0\right) \end{array} \tag{6}$$

2.2.2. Constitutive Relations

Considering that a functionally graded material can be considered as an isotropic material at each point, the constitutive relation for the present model can be written as [36]

$$\begin{array}{c} \sigma_x = Q_{11}\varepsilon_x \\ \sigma_{xz} = Q_{55}\gamma_{xz} \end{array} \tag{7}$$

with the elastic stiffness coefficients, which may depend either on the thickness or on the length coordinates, being given as

$$\begin{array}{c} Q_{11} = E_{FGM}(x,z) \\ Q_{55} = \frac{E_{FGM}(x,z)}{2(1+\nu_{FGM}(x,z))}ks \end{array} \tag{8}$$

with ks being the shear correction factor, which in the present study was set to 5/6. This value was selected because the references considered in the verification cases also considered it and because although the material distribution can affect this factor, this value is widely adopted in published works. However, this factor can also be calculated as for example in [37–40].

The stress resultants [41] will be defined as

$$(N_x, M_x) = \int_A (1, z)\sigma_x dA; \;\; Q_{xz} = \int_A \sigma_{xz} dA \tag{9}$$

which by considering the constitutive relation and the generalized strains, yield the following:

$$\begin{array}{c} \begin{bmatrix} N_x \\ M_x \end{bmatrix} = \begin{bmatrix} A_{11} & B_{11} \\ B_{11} & C_{11} \end{bmatrix} \begin{bmatrix} \frac{\partial u^0}{\partial x} \\ \frac{\partial \theta_x^0}{\partial x} \end{bmatrix}; \;\; [Q_{xz}] = [A_{55}]\left[\frac{\partial w^0}{\partial x} + \theta_x^0\right] \\ (A_{11} \;\; B_{11} \;\; D_{11}) = \int_A Q_{11}\left(1 \;\; z \;\; z^2\right) dA; \;\; ; \;\; (A_{55}) = \int_A Q_{55}\, dA \end{array} \tag{10}$$

with A standing for the beam' transverse cross-section area.

2.2.3. Equilibrium Equations

The equilibrium equations are derived through Hamilton's principle [42]:

$$\delta \int_{t1}^{t2} (T - (U + \Omega))\, dt = 0 \tag{11}$$

where δT, δU and δΩ denote the variations of the kinetic energy, of the elastic strain energy and of the external forces' potential energy, respectively. Carrying out the integration in the cross-section area, they can be written as

$$\delta T = \int_0^l \left(I_0 \dot{u^0} \delta \dot{u^0} + I_1 \dot{u^0} \delta \dot{\theta_x^0} + I_1 \dot{\theta_x^0} \delta \dot{u^0} + I_2 \dot{\theta_x^0} \delta \dot{\theta_x^0} + I_0 \dot{w^0} \delta \dot{w^0} \right) dx \tag{12}$$

$$\delta U = \int_0^l \left(\frac{\partial}{\partial x} N_x \delta u^0 + \left(\frac{\partial}{\partial x} M_x + Q_{xz} \right) \delta \theta_x^0 + \frac{\partial}{\partial x} Q_{xz} \delta w^0 \right) dx \tag{13}$$

where $(\cdot)$ denotes the first time derivative. As one aims to consider free-vibration analyses, we will only have these two terms. The Hamilton principle, thus, leads to the equations:

$$\begin{array}{c} \delta u: \ I_0\ddot{u^0} + I_1\ddot{\theta}_x = \frac{\partial N_x}{\partial x} \\ \delta\theta_x: \ I_1\ddot{u^0} + I_2\ddot{\theta}_x = \frac{\partial M_x}{\partial x} + Q_{xz} \\ \delta w: \ I_0\ddot{w} = \frac{\partial Q_{xz}}{\partial x} - q_z \end{array} \tag{14}$$

with $(\cdot\cdot)$ standing for the second time derivative. The mass moments of inertia, I_k, are given as $(I_0\ I_1\ I_2) = \int_A \rho\left(1\ z\ z^2\right)\ dA$ with ρ standing for the density. A possible transversely distributed load is represented by q_z, which will be null as one aims at performing free-vibration analyses.

As stated by Eringen [2,3], the stress field at a specific point in an elastic continuum body also depends on the strains at all other points of that body, as given in Equation (15):

$$\left(1 - \mu\nabla^2\right)\sigma = t; \ \ \mu = (e_0 a)^2 \tag{15}$$

where σ is the stress tensor at a generic point x, and t is the macroscopic stress tensor at that point. μ represents the nonlocal parameter, and it is a function of the material constant e_0 and the characteristic length a. Expanding Equation (15) for the present model, one will achieve the corresponding nonlocal constitutive relation:

$$\begin{array}{c} \sigma_x - \mu\frac{\partial^2}{\partial x^2}\sigma_x = Q_{11}\varepsilon_x \\ \sigma_{xz} - \mu\frac{\partial^2}{\partial x^2}\sigma_{xz} = Q_{55}\gamma_{xz} \end{array} \tag{16}$$

and accordingly, the stress resultants will be expressed by

$$\begin{array}{c} N_x - \mu\frac{\partial^2}{\partial x^2}N_x = A_{11}\frac{\partial u^0}{\partial x} + B_{11}\frac{\partial\theta_x^0}{\partial x} \\ M_x - \mu\frac{\partial^2}{\partial x^2}M_x = B_{11}\frac{\partial u^0}{\partial x} + C_{11}\frac{\partial\theta_x^0}{\partial x} \\ Q_{xz} - \mu\frac{\partial^2}{\partial x^2}Q_{xz} = A_{55}\left(\frac{\partial w^0}{\partial x} + \theta_x^0\right) \end{array} \tag{17}$$

Considering these relations and the equations of motion, after some mathematical manipulation one can write

$$\begin{array}{rl} \delta U = \int_0^l (& A_{11}\frac{\partial u^0}{\partial x}\frac{\partial\delta u^0}{\partial x} + B_{11}\frac{\partial\theta_x^0}{\partial x}\frac{\partial\delta u^0}{\partial x} + C_{11}\frac{\partial\phi_x^0}{\partial x}\frac{\partial\delta u^0}{\partial x} + B_{11}\frac{\partial u^0}{\partial x}\frac{\partial\delta\theta_x^0}{\partial x} \\ & + C_{11}\frac{\partial\theta_x^0}{\partial x}\frac{\partial\delta\theta_x^0}{\partial x} + A_{55}\frac{\partial w^0}{\partial x}\frac{\partial\delta w^0}{\partial x} + A_{55}\theta_x^0\frac{\partial\delta w^0}{\partial x} + A_{55}\theta_x^0\delta\theta_x^0 \\ & + A_{55}\frac{\partial w^0}{\partial x}\delta\theta_x^0\Big)dx \end{array} \tag{18}$$

$$\delta T = \int_0^l \left(1 - \mu\frac{\partial^2}{\partial x^2}\right)\left(I_0\ddot{u}\delta u^0 + I_1\ddot{\theta}_x\delta u^0 + I_0\ddot{w}\delta w^0 + I_1\ddot{u}\delta\theta_x^0 + I_2\ddot{\theta}_x\delta\theta_x^0\right)dx \tag{19}$$

which allows one to obtain and implement the nonlocal FSDT beam model considering free and harmonic vibrations.

The finite element method is used to implement and perform the free-vibration analyses using a quadratic beam finite element (three nodes) with three degrees of freedom per node, namely $\{u^0, w^0, \theta_x^0\}$. According to the finite element method, the generalized displacements will be described as linear combinations of the corresponding nodal degrees of freedom and the nodal shape functions. Strains will be obtained accordingly by considering Equation (6). Considering this and Equations (11), (18) and (19), one obtains the equilibrium equation at the element level [36].

$$\left(K^e - \omega_i^2 M^e\right)q_i = 0 \tag{20}$$

with K^e and M^e standing for the stiffness and mass matrices of the e-th element, and q_i representing the vibration mode for the i-th natural vibration frequency ω_i.

Considering the contribution of the elements that will jointly constitute the whole discretized domain and after the boundary conditions' imposition, one will achieve the reduced system that will allow the eigenvalues and corresponding eigenvectors to be obtained [43]. Finally, one will determine the structure's frequencies and respective vibration modes.

A schematic description of the analysis procedure is provided below:

Declaration of variables
Selection of volume fraction law (Equation (1) or Equation (2)
Selection of Voigt's rule equation (Equation (3) or Equation (4))
Constitution of the discretized domain
Calculation of reduced stiffness coefficients (Equation (8))
For each set of parameters $\left(\mu,\ \frac{L}{h},\ p_x,\ p_z,\ FGM1,\ FGM2\right)$, *perform the following:*

Calculation of element stiffness matrix (associated to Equation (18))
Calculation of element mass matrix (associated to Equation (19))
Assembly of the element matrices into the global matrices
Imposition of boundary conditions
Calculation of eigenproblem solution (Equation (20))
Calculation of natural frequencies
Vibration modes' representation

with the natural frequencies being obtained from the square root of the eigenvalues obtained.

3. Results and Discussion

The first two cases here presented are verification cases, whose objective is to demonstrate the performance of the developed beam finite element model and to assess its convergence. In the first verification case, a local approach is used to assess the behaviour of an FGM beam, and in the second verification case, the nonlocal approach that will be used in the following case studies is also compared with alternative nonlocal results.

Following the verification cases, a set of parametric studies is considered to characterize the influence of specific parameters on the free vibrations' nonlocal response of simply supported (SS) metallic FGM beams.

The simply supported boundary conditions correspond to the following restrictions: in the discretized domain's first node (left-hand side of the beam), the constrained displacements are $\{u^0, w^0\}$, and at the domain' final node (right-hand side of the beam), the constrained displacement is $\{w^0\}$.

3.1. Model Verification

3.1.1. Verification Case 1

A first verification study was carried out to assess the present model's performance concerning the free vibration of functionally graded beams, taking as reference Sina et al. [42], who used Timoshenko beam theory, and Simsek [43], who considered different shear deformation models. A pinned–pinned aluminium–alumina FGM1-Z beam with a length-to-thickness ratio of 10 and with the exponent pz $=$ 0.3 was analysed. The material properties of the two constituent phases used by the references were as follows: for the aluminium E $=$ 70 GPa, $\nu = 0.23$, $\rho = 2700\ \mathrm{kg.m^{-3}}$ and for the alumina E $=$ 380 GPa, $\nu = 0.23$, $\rho = 3800\ \mathrm{kg.m^{-3}}$. This case was also used for convergence test purposes.

The nondimensional results in Table 1 were obtained by using the multiplier $\Omega_{adim} = \Omega L^2\sqrt{\frac{I_0}{EI}}$, where I_0 stands for $\int_{-h/2}^{h/2} \rho_{FGM} dz$ and $EI = h^2 \int_{-h/2}^{h/2} E_{FGM} dz$.

Table 1. Nondimensional fundamental frequency Ω_{adim} of metal–ceramic FGM beam. Convergence test.

			Elements			
L/h	**Sina et al. [42]**	**Simsek [43] (FSDBT)**	**5**	**10**	**15**	**20**
10	2.695	2.701	2.703	2.702	2.702	2.702
30	2.737	2.738	2.739	2.738	2.738	2.738
100	2.742	2.742	2.743	2.743	2.743	2.743

As one can conclude from Table 1, even with coarse meshes, good agreement was obtained with Simsek [43] and with Sina et al. [42]. Based on that, and although with five elements the results are also in good agreement, we decided to proceed with a ten elements' discretization for the next case studies.

3.1.2. Verification Case 2

This verification case is focused now on the characterization of the nondimensional fundamental frequencies of simply supported beams (SS) using Eringen's nonlocal theory. To this purpose, the work developed by Reddy [1] was taken as the reference. According to the reference, the beam parameters used were length of the beam L = 10, elasticity modulus and Poisson's ratio $E = 30 \times 10^6$ and $\nu = 0.3$, and a unitary density ρ. The nondimensional frequencies were obtained by using the expression $\Omega_{adim} = \Omega L^2 \sqrt{\frac{I_0}{EI}}$ and are presented in Table 2 for two length-to-thickness ratios.

Table 2. Nondimensional fundamental frequencies (Ω_{adim}) in SS homogeneous beams.

	L/h = 100			**L/h = 10**		
μ	**TBT [1]**	**FSDT**	**Dev %**	**TBT [1]**	**FSDT**	**Dev %**
0	9.8683	9.8183	−0.507	9.7454	9.6602	−0.874
0.5	9.6335	9.5847	−0.507	9.5135	9.4303	−0.875
1	9.4147	9.367	−0.507	9.2973	9.2161	−0.873
1.5	9.2101	9.1634	−0.507	9.0953	9.0159	−0.873
2	9.0183	8.9726	−0.507	8.9059	8.8282	−0.872
2.5	8.838	8.7933	−0.506	8.7279	8.6517	−0.873
3	8.6682	8.6243	−0.506	8.5601	8.4854	−0.873
3.5	8.5077	8.4646	−0.507	8.4017	8.3283	−0.874
4	8.3558	8.3135	−0.506	8.2517	8.1797	−0.873
4.5	8.2118	8.1703	−0.505	8.1095	8.039	−0.869
5	8.075	8.0342	−0.505	7.9744	7.9048	−0.873

From Table 2, one can also observe a good agreement between the results obtained by the present model and the ones in [1] for both aspect ratios.

3.2. Parametric Case Studies

Following the previous verification cases, a set of parametric studies was carried out to characterize the influence of different parameters on the predictions for nonlocal natural frequencies of aluminium–cadmium simply supported beams.

The nonlocal parameter may assume scattered values as one can find in literature, however for similar situations, such as the ones in [1,39,40] one finds values between 1 and 5. Hence, it was decided to carry out the case studies within the range $0 \leq \mu \leq 3$. The material properties of the two constituent phases for these parametric studies were, for the cadmium, $E = 55.2$ GPa, $\nu = 0.33$, $\rho = 8640$ kg.m^{-3} and, for the aluminium, $E = 68.3$ GPa, $\nu = 0.34$, $\rho = 2690$ kg.m^{-3}. This case was also used for convergence test purposes.

The case studies are organized according to the following structure:

- Nondimensional fundamental frequencies of FGM1-Z beams;
- Nondimensional fundamental frequencies of FGM1-X beams;
- Nondimensional first three natural frequencies of FGM1 beams;
- Nondimensional first three natural frequencies of FGM2 beams.

The first two cases are focused in the nondimensional fundamental frequencies of the beams of a specific type of FGM in which the aluminium phase is progressively mixed with the cadmium phase. The aim here was to carry out detailed studies for a single type of FGM (FGM1 selected for that purpose), wherein the mixture progresses according to two different directions' volume fraction distribution laws along Z or X direction (Equations (1) and (2)).

In the last two case studies, both types of FGMs were considered to illustrate how each one influenced the beams' higher-order frequencies. This was done in a first stage for the FGM1 type of beams and in a second stage for the FGM2 one. A set of parametric analyses were conducted for comparative purposes and to highlight the differences among the constructive solutions.

3.2.1. Case 1—Nondimensional Fundamental Frequencies of FGM1-Z SS Beams

The first study considers simply supported beams in which the material mixture is ruled by the power law FGM1-Z (Equations (1) and (3)). Two length-to-thickness ratios and a set of pz exponent values are considered to analyse the influence of the nonlocal parameter in the fundamental frequencies Ω.

The results obtained are presented in Table 3 in a nondimensional manner, using $\Omega_{adim} = \Omega L^2 \sqrt{\frac{I_{0Al}}{E_{Al}I}}$ with $I_{0Al} = \int_A \rho_{Al} dA$.

Table 3. Nondimensional fundamental frequencies (Ω_{adim}) of SS FGM1-Z beams.

		pz					
	μ	**0**	**0.1**	**0.5**	**1**	**2**	**10**
L/h = 10	**0**	9.657	8.734	7.064	6.315	5.759	5.100
	1.0	9.213	8.333	6.739	6.024	5.494	4.865
	2.0	8.825	7.982	6.455	5.771	5.263	4.661
	3.0	8.482	7.672	6.205	5.547	5.058	4.480
L/h = 30	**0**	9.801	8.866	7.171	6.410	5.845	5.176
	1.0	9.748	8.818	7.132	6.375	5.813	5.148
	2.0	9.696	8.770	7.093	6.341	5.782	5.120
	3.0	9.644	8.724	7.055	6.307	5.751	5.093

In this case (FGM1-Z), as the exponent pz increases, the material becomes less stiff and the mass increases. From this trade-off, we can observe that the nondimensional frequencies decrease as the exponent increases. This trend is verified for both aspect ratios. The slender beam presents greater nondimensional frequencies, which is expected considering the multiplier used. The nonlocal parameter was found to introduce a decreasing effect on the nondimensional fundamental frequencies. Figure 2 presents the ratio $\left(\frac{\Omega_{adim}^{FGM1-Z}}{\left(\Omega_{adim}^{FGM1-Z}\right)_{\mu=0}}\right)$ between nonlocal fundamental frequencies and the corresponding local ones ($\mu = 0$) for the FGM1-Z thicker beams. The ratio is presented for different values of *pz* exponent $\{0, 0.1, 0.5, 1, 2, 10\}$.

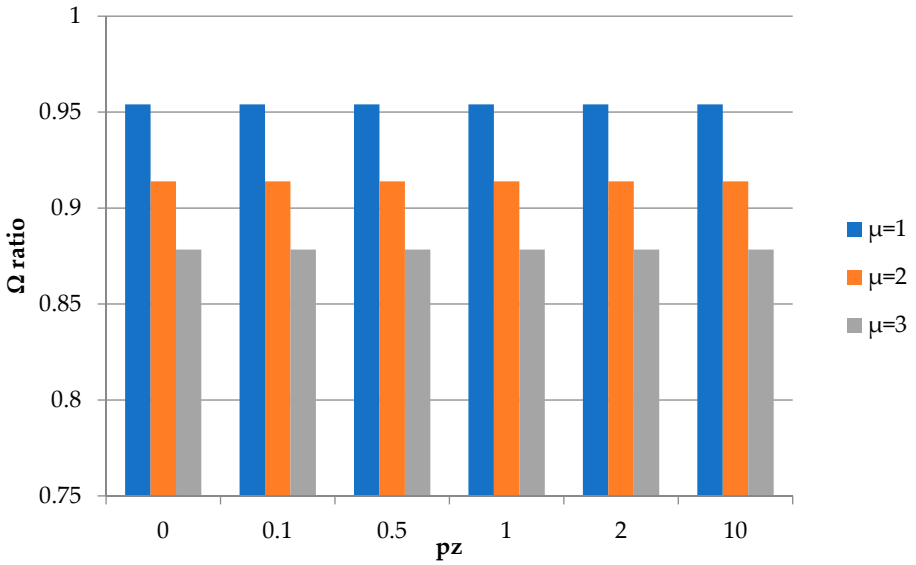

Figure 2. Ratios $\left(\frac{\Omega_{adim}^{FGM1-Z}}{\left(\Omega_{adim}^{FGM1-Z}\right)_{\mu=0}}\right)$ between nondimensional nonlocal and local fundamental frequencies for FGM1-Z, SS beams. L/h = 10.

The figure clearly represents the increasingly reducing effect that the increase in the nonlocal parameter μ has in the nondimensional fundamental frequency, being clearly visible for any exponent value. This reduction assumes a 4.6% value for $\mu = 1$ and 12.2% for $\mu = 3$, taking as reference the nondimensional local prediction ($\mu = 0$).

3.2.2. Case 2—Nondimensional Fundamental Frequencies of FGM1-X Beams

Here, we develop a study similar to the one carried out in the previous case; however, now, the object of study is FGM1-X, SS beams. The influences of the length-to-thickness ratio, of the *px* exponent (Equations (2) and (3)) and of the nonlocal parameter are considered.

The nondimensional results are presented in Table 4, using the multiplier defined in the previous case study.

Table 4. Nondimensional fundamental frequencies (Ω_{adim}) of SS FGM1-X beams.

		px					
	μ	**0**	**0.1**	**0.5**	**1**	**2**	**10**
L/h = 10	**0**	9.657	8.316	6.352	5.622	5.162	4.861
	1.0	9.213	7.995	6.152	5.447	4.991	4.662
	2.0	8.825	7.708	5.970	5.288	4.836	4.485
	3.0	8.482	7.450	5.802	5.141	4.695	4.327
L/h = 30	**0**	9.801	8.434	6.436	5.694	5.229	4.930
	1.0	9.748	8.396	6.412	5.674	5.209	4.906
	2.0	9.696	8.359	6.389	5.654	5.189	4.882
	3.0	9.644	8.322	6.366	5.634	5.170	4.859

In this case, and according to the volume fraction expression in Equation (2) and the rule of mixtures in Equation (3), we see that as the exponent *px* increases, the Young's modulus value will decrease in the major part of the beam length only retaining the higher value for aluminium near the beam extremities. The density evolution presents the opposite profile.

In correspondence with these properties' profiles, one concludes that the nondimensional frequencies decrease with the exponent increase and the corresponding stiffness reduction. The nonlocal parameter introduces a visible reducing influence for all the exponents.

This decreasing effect due to nonlocal parameter increase is also illustrated through the ratio $\left(\frac{\Omega_{adim}^{FGM1-X}}{(\Omega_{adim}^{FGM1-X})_{\mu=0}}\right)$ established between nonlocal fundamental frequencies and the corresponding local ones ($\mu = 0$) presented in Figure 3. As we observe, this ratio does not follow a uniform reducing pattern for the different exponent values as happened in the previous case study, with this effect being greater when the mixture is globally less heterogeneous as one may conclude from Figures A3 and A4.

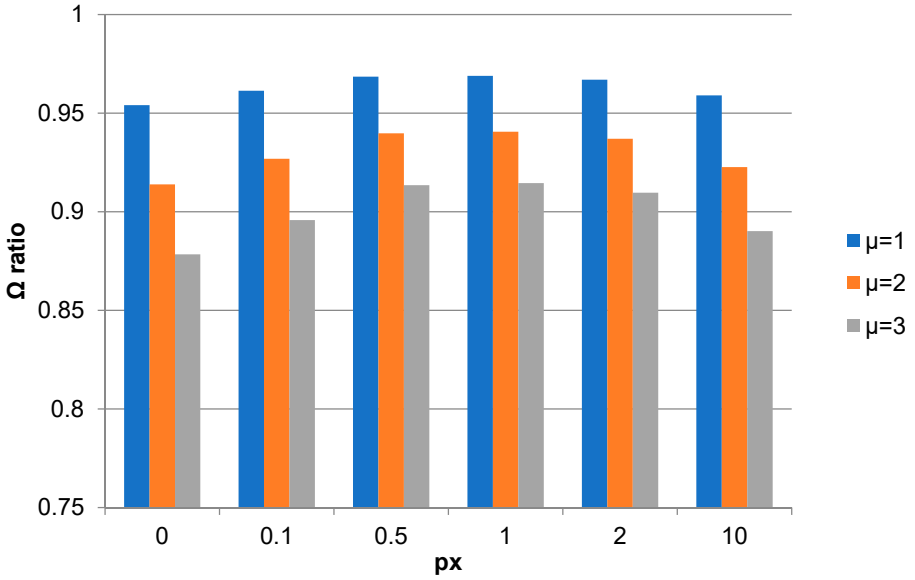

Figure 3. Ratios $\left(\frac{\Omega_{adim}^{FGM1-X}}{(\Omega_{adim}^{FGM1-X})_{\mu=0}}\right)$ between nondimensional nonlocal and local fundamental frequencies for FGM1-X, SS beams. L/h = 10.

For the considered domains, the greater reducing influence occurs for the null *px* exponent for all the nonlocal parameters, assuming this reduction at a 12.2% value for $\mu = 3$.

For different nonlocal parameter values (μ = 1–3), the nondimensional frequencies suffer minor reductions for the exponent value px = 1, varying from 3.1% for $\mu = 1$ to 8.6% for $\mu = 3$.

3.2.3. Case 3—Nondimensional First Three Natural Frequencies of FGM1 Beams

In this case, one proceeds to a comparative analysis of the first three nondimensional natural frequencies of the FGM1-Z and FGM1-X beams. The material and geometric characteristics remain constant. The results obtained are presented in Table 5.

Table 5 allows the conclusion that the FGM1-X configuration has a greater impact in the nondimensional frequencies' reduction than the FGM1-Z, taking as reference the homogeneous aluminium beam (null exponent). Figure 4 illustrates the first three vibration modes for this case.

Table 5. Nondimensional first three natural frequencies (Ω_{adim}) of SS FGM1-Z and FGM1-X beams. L/h = 10.

				pz				***px***	
μ	**0**	**1**	**2**	**5**	**10**	**1**	**2**	**5**	**10**
0	9.657	6.315	5.759	5.306	5.100	5.622	5.162	4.910	4.861
	36.887	24.113	21.993	20.266	19.483	24.056	21.263	19.247	18.720
	54.413	35.638	32.277	29.543	28.437	35.501	32.185	29.517	28.460
1	9.213	6.024	5.494	5.062	4.865	5.447	4.991	4.725	4.662
	31.234	20.419	18.625	17.161	16.497	20.305	18.172	16.564	16.058
	53.754	35.163	31.852	29.171	28.087	35.060	31.785	29.152	28.111
2	8.825	5.771	5.263	4.849	4.661	5.288	4.836	4.560	4.485
	27.575	18.028	16.443	15.151	14.565	17.886	16.122	14.755	14.279
	46.642	30.476	27.801	25.622	24.635	30.412	27.492	25.235	24.374
3	8.482	5.547	5.058	4.660	4.480	5.141	4.695	4.410	4.327
	24.959	16.318	14.884	13.714	13.183	16.163	14.636	13.431	12.984
	40.597	26.532	24.204	22.304	21.443	26.459	23.940	22.019	21.274

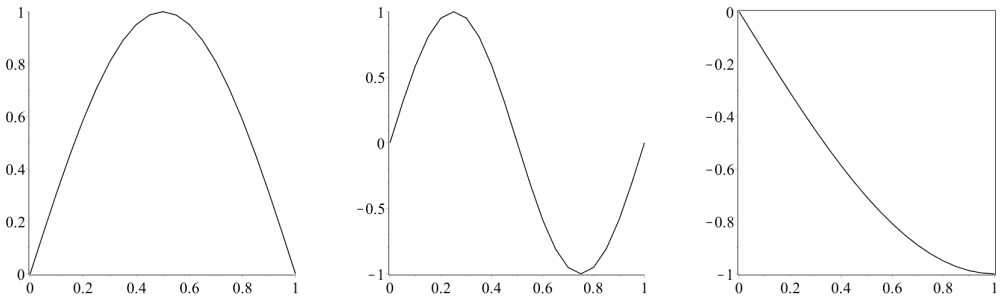

Figure 4. FGM1 beams' vibration modes: (**a**) first mode, (**b**) second mode, (**c**) third mode. L/h = 10.

From Table 5, it can also be concluded that with the increase in the nonlocal parameter μ, the three nondimensional natural frequencies decrease, as already observed in the case of the nondimensional fundamental frequency.

Figure 5 complementarily illustrates for the FGM1-Z that for higher modes' frequencies the decreasing effect associated with the nonlocal parameter is more evident and increases with the mode. This is also visible for the effect of the *pz* exponent within each mode.

Figure 6 depicts the curves for the ratios $\left(\frac{\Omega_{adim}^{FGM1-X}}{\Omega_{adim}^{FGM1-Z}}\right)$, denoting the relations between the nondimensional fundamental frequencies of FGM1-X and FGM1-Z beams for different exponent values.

From Figure 6, one observes that as the nonlocal parameter grows, the ratio between the two material models becomes closer to 1 in opposition to the local approach ($\mu = 0$). It is also visible that, for globally less homogeneous mixtures, which are the case of the intermediate exponents, the frequency differences between the FGM1-X and FGM1-Z models are greater as the nature of the distribution acquires a greater influence.

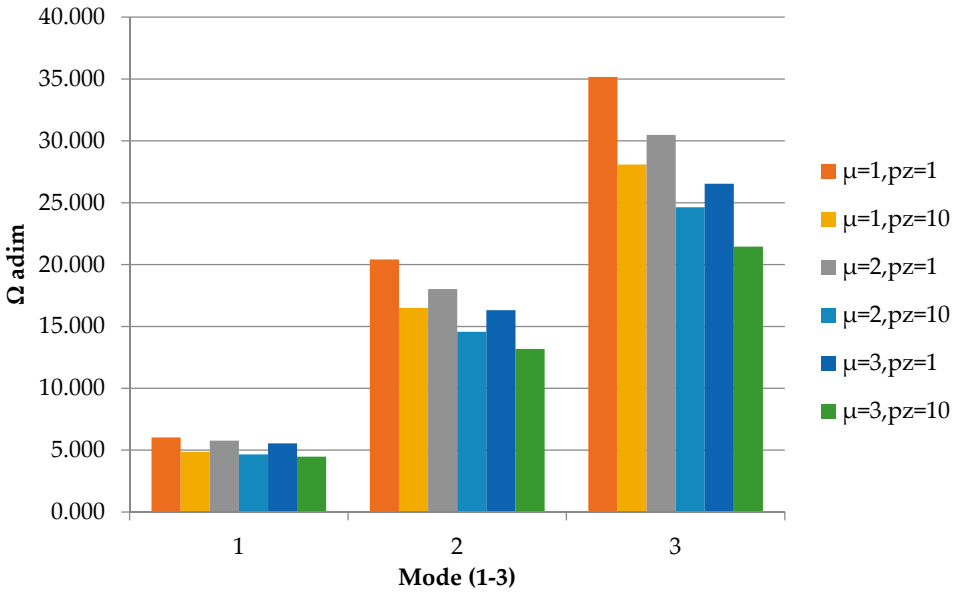

Figure 5. FGM1-Z nondimensional frequencies (Ω_{adim}) for different vibration modes. L/h = 10.

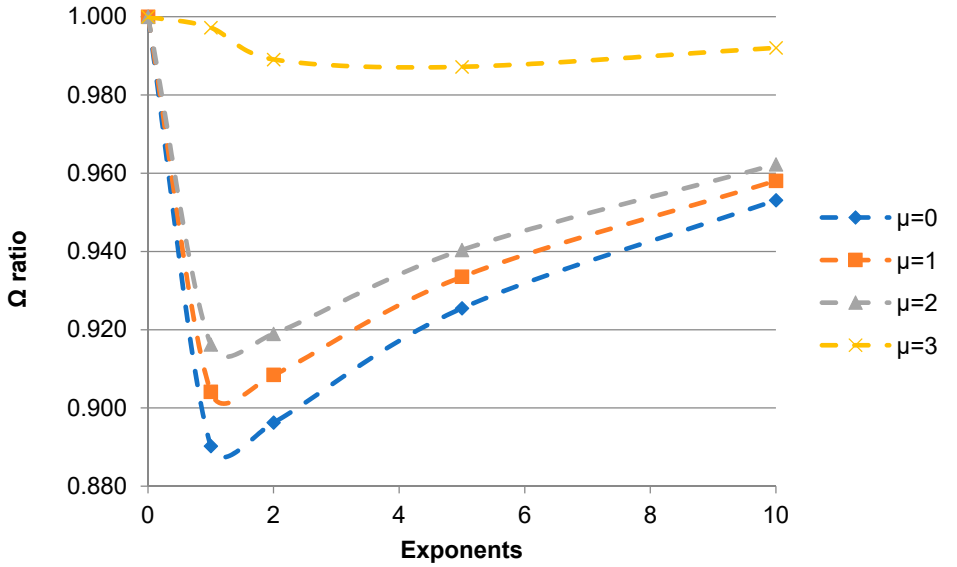

Figure 6. Ratios $\left(\frac{\Omega_{adim}^{FGM1-X}}{\Omega_{adim}^{FGM1-Z}}\right)$ between nondimensional fundamental frequencies for FGM1-X and FGM1-Z beams. L/h = 10.

The differences identified previously concerning the ratios between nondimensional nonlocal and local fundamental frequencies are here reflected by the curve profiles with respect to ratio behaviour near the 1, 2 exponents' values.

From the results achieved in this case, it can be said that FGM1-Z beams perform globally better than FGM1-X ones.

3.2.4. Case 4—Nondimensional First Three Natural Frequencies of FGM2 Beams

This case study now considers the FGM2 material models and proceeds with the comparative analyses of the first three nondimensional natural frequencies of those beams. The material and geometric characteristics are the same as well as the boundary conditions used previously. The mixture of the constituent materials is now ruled by Equation (4), and this significantly affects the beams' response. As expected, the beams now become globally stiffer as the exponents increase, and this is reflected by greater nondimensional frequencies as observed in Table 6. Those results were obtained using $\Omega_{adim} = \Omega L^2 \sqrt{\frac{I_{0Cd}}{E_{Cd} I}}$ with $I_{0Cd} = \int_A \rho_{Cd} dA$.

Table 6. Nondimensional first three natural frequencies (Ω_{adim}) of SS FGM2-Z and FGM2-X beams. L/h = 10.

				pz				*px*	
μ	**0**	**1**	**2**	**5**	**10**	**1**	**2**	**5**	**10**
0	9.657	12.589	14.018	16.017	17.310	14.432	16.644	18.601	19.088
	36.900	48.069	53.502	61.105	66.047	47.956	55.576	66.735	19.088
	54.413	71.046	79.634	91.369	98.507	70.772	79.164	90.790	97.860
1	9.214	12.010	13.373	15.281	16.514	13.447	15.403	17.295	17.913
	31.245	40.706	45.306	51.742	55.926	40.479	46.004	53.864	57.957
	53.754	70.099	78.552	90.178	97.279	69.894	78.178	89.660	96.647
2	8.826	11.504	12.810	14.637	15.819	12.639	14.403	16.227	16.929
	27.584	35.939	40.000	45.681	49.374	35.656	40.092	46.327	49.954
	46.673	60.755	67.589	77.157	83.410	60.772	67.839	76.585	81.939
3	8.483	11.058	12.313	14.069	15.205	11.961	13.575	15.334	16.090
	24.967	32.530	36.206	41.348	44.690	32.221	35.986	41.248	44.530
	40.624	52.893	58.842	67.165	72.604	52.643	58.774	66.255	70.678

In this case, when the exponents assume the zero value, one has a homogeneous cadmium beam. The nonlocal parameter continues to show a decreasing effect in the nondimensional frequencies, with this influence being greater as the exponents increase. Their effect is also greater for higher modes' frequencies. This is visible in Figures 7 and 8.

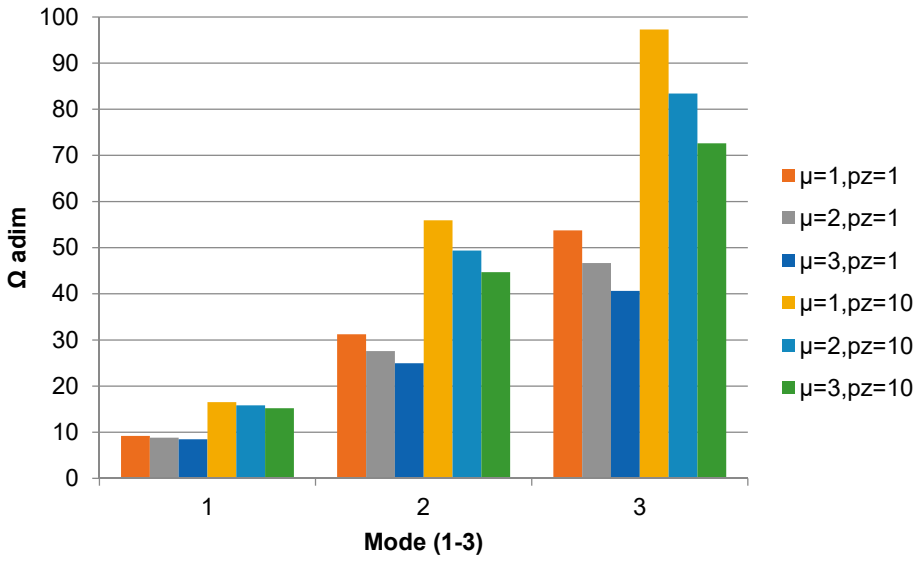

Figure 7. FGM2-Z nondimensional frequencies (Ω_{adim}) for different vibration modes. L/h = 10.

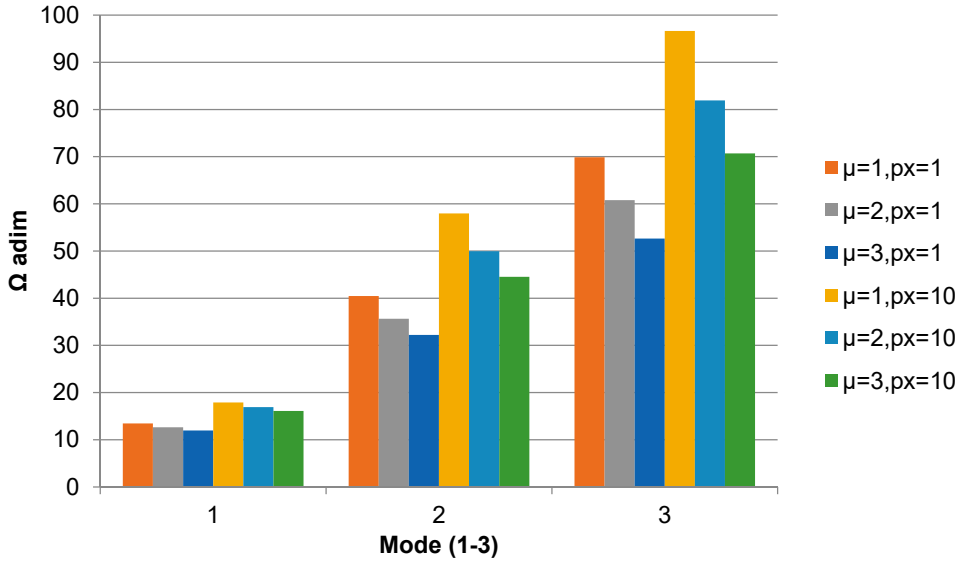

Figure 8. FGM2-X nondimensional frequencies (Ω_{adim}) for different vibration modes. L/h = 10.

Table 6 and also Figure 9 allow the conclusion that the beams with a non-null gradient mixture along their length (FGM2-X) show greater nondimensional frequencies when compared with the FGM2-Z beams. In such a situation, one obtains ratios for the nondimensional fundamental frequencies that range from 15% to 19% within the exponents' set $\{1, 2, 5\}$.

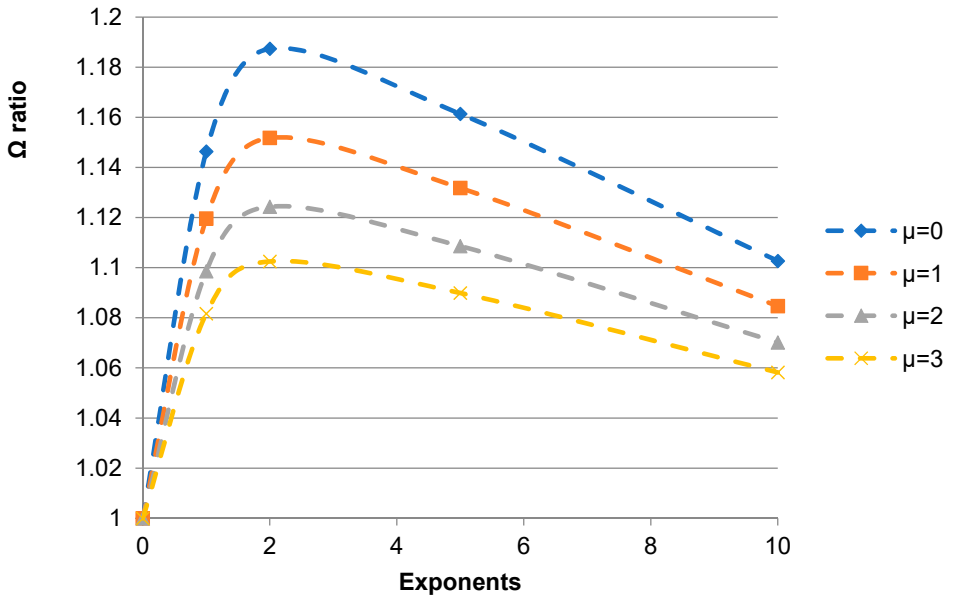

Figure 9. Ratios $\left(\frac{\Omega_{adim}^{FGM2-X}}{\Omega_{adim}^{FGM2-Z}}\right)$ between nondimensional fundamental frequencies for FGM2-X and FGM2-Z beams. L/h = 10.

For the nonlocal parameter μ. values $\{1, 2, 3\}$, this ratio decreases, successively assuming the maximum values 15%, 12% and 10%, respectively.

As we previously concluded, as μ increases, the differences between the predicted frequencies start to present a decreasing trend.

For the second mode, the nondimensional frequencies ratios are not so high, but for the nonlocal parameter values $\{0, 1, 2, 3\}$, one achieves maximum values of 9.2%, 4.1%, 1.4% and 1% for the exponents $\{5, 5, 5, 1\}$, respectively.

In the third mode case, the ratio maximum values occur for the maximum exponent considered, assuming successively the values 0.7%, 0.6%, 1.8% and 2.7%, as the nonlocal parameter goes from 0 to 3.

It can, thus, be said that, for the studied parameter domain, FGM2-X beams present a better performance when compared to the corresponding FGM2-Z ones.

As a final note, if one considered the use of the multiplier used in the previous case studies, $\Omega_{adim} = \Omega L^2 \sqrt{\frac{I_{0Al}}{E_{Al} I}}$. with $I_{0Al} = \int_A \rho_{Al} dA$, where the elastic properties of the aluminium phase are used, the present case nondimensional frequencies will globally present lower values when compared with the ones in Table 6, as can be seen in Table 7, although maintaining the same trends. This is expected considering the relation between the material properties used in the two multipliers.

Table 7. Nondimensional first three natural frequencies (Ω_{adim}) of SS FGM2-Z and FGM2-X beams, using aluminium as reference. L/h = 10.

				pz				***px***	
μ	**0**	**1**	**2**	**5**	**10**	**1**	**2**	**5**	**10**
0	4.844	6.315	7.032	8.034	8.683	7.239	8.349	9.331	9.575
	18.510	24.113	26.838	30.652	33.131	24.056	27.878	33.476	9.575
	27.295	35.638	39.946	45.833	49.413	35.501	39.710	45.542	49.089
1	4.622	6.024	6.708	7.665	8.284	6.745	7.727	8.676	8.986
	15.673	20.419	22.727	25.955	28.054	20.305	23.077	27.020	29.073
	26.964	35.163	39.403	45.236	48.798	35.060	39.216	44.976	48.480
2	4.427	5.771	6.426	7.342	7.935	6.340	7.225	8.140	8.492
	13.837	18.028	20.065	22.915	24.767	17.886	20.111	23.239	25.058
	23.412	30.476	33.904	38.704	41.841	30.485	34.030	38.417	41.102
3	4.255	5.547	6.176	7.057	7.627	6.000	6.810	7.692	8.071
	12.524	16.318	18.162	20.741	22.418	16.163	18.052	20.691	22.337
	20.378	26.532	29.517	33.691	36.420	26.407	29.483	33.235	35.454

However, when one considers the relation between these nondimensional values (corresponding to the FGM2 beams) and the analogous ones in Table 5 (corresponding to the FGM1 beams), we achieve the results presented in Table 8.

Table 8. Relation between nondimensional first three natural frequencies (Ω_{adim}) of SS FGM2 and FGM1 beams, using aluminium as reference. L/h = 10.

				pz				***px***	
μ	**0**	**1**	**2**	**5**	**10**	**1**	**2**	**5**	**10**
0	0.502	1	1.221	1.514	1.703	1.288	1.617	1.900	1.970
	0.502	1	1.220	1.512	1.701	1.000	1.311	1.739	0.511
	0.502	1	1.238	1.551	1.738	1.000	1.234	1.543	1.725
1	0.502	1	1.221	1.514	1.703	1.238	1.548	1.836	1.927
	0.502	1	1.220	1.512	1.701	1.000	1.270	1.631	1.810
	0.502	1	1.237	1.551	1.737	1.000	1.234	1.543	1.725
2	0.502	1	1.221	1.514	1.702	1.199	1.494	1.785	1.893
	0.502	1	1.220	1.512	1.700	1.000	1.247	1.575	1.755
	0.502	1	1.220	1.511	1.698	1.002	1.238	1.522	1.686
3	0.502	1	1.221	1.514	1.702	1.167	1.450	1.744	1.865
	0.502	1	1.220	1.512	1.701	1.000	1.233	1.541	1.720
	0.502	1	1.220	1.511	1.698	0.998	1.232	1.509	1.667

These results allow us to conclude that FGM2 beams in a majority of situations can provide higher values of nondimensional frequencies when compared to FGM1 beams. The decreasing effect of the nonlocal parameter is also visible here.

4. Conclusions

This work presented a study on the free-vibration response of simply supported beams made of through-thickness and lengthwise metal–metal functionally graded materials, taking into account nonlocal effects. In order to assess the influence that size-dependent effects introduce on free-vibration responses, the first-order shear deformation theory and the Eringen' nonlocal elasticity theory were considered.

The metallic phases involved were aluminium and the cadmium due to its chemical compatibility and also due to the improvement in terms of corrosion and wear resistance according to recent investigation. Taking into account the boundary conditions of the beams to be studied, two material-phase mixture laws were adopted; namely the known power law and another mixture distribution, proposed in the present study.

The beam model's performance was verified with alternative solutions, demonstrating its good agreement in the considered domains. The influence of parameters such as the beams' aspect ratios, the evolution of the constituents' mixture and the influence of the nonlocal parameter of Eringen' theory were analysed, and conclusions were drawn with respect to their better relative performance.

It was found that, for the FGM1-type beams, for which the null exponent corresponded to a full-aluminium beam, with the mixture evolution along the thickness direction, FGM1-Z, produced a minor decrease in the nondimensional frequencies when compared with the beams with a material distribution along the length, FGM1-X, for the same exponents. For the other beams, the FGM2-type beams, for which the null exponent corresponded to a full-cadmium beam and as expected, the opposite trend was observed. For similar exponents, the FGM2-X presents higher nondimensional frequencies when compared to the FGM2-Z.

It was also possible to conclude that the nonlocal effects introduced a decreasing influence in the natural frequencies, regardless of the frequency mode, which corresponds to an expected trend. This effect was found to be influenced by the exponents associated with the metals' mixture profiles.

The nondimensional frequencies increased with the aspect ratio increase, agreeing with other authors results, and regardless of the aspect ratio value considered, the decreasing effect in the nondimensional frequencies due to the increase in the nonlocal parameter was evident.

The relation between the nondimensional frequencies of FGM2 and FGM1 beams, allows the understanding that the first ones provide higher values, with a decreasing trend for higher nonlocal parameter values.

As an overall conclusion, it can be stated that the proposed materials' lengthwise distribution can be an effective design option to consider as it is able to provide an improved free-vibration response.

Author Contributions: M.A.R.L.: conceptualization, methodology, software, validation and writing—original draft. K.R.: conceptualization, writing—review and editing and visualization. J.I.B.: conceptualization, resources, methodology and visualization. All authors have read and agreed to this manuscript version.

Funding: This research received no external funding.

Institutional Review Board Statement: Not applicable.

Informed Consent Statement: Not applicable.

Data Availability Statement: Not applicable.

Acknowledgments: The authors wish to acknowledge the support given by FCT, through IDMEC, under LAETA, project UIDB/50022/2020.

Conflicts of Interest: The authors declare no conflict of interest.

Appendix A

In this appendix, the Young's modulus and the density evolutions through the beam thickness and along the beam length are presented with a complementary illustrative purpose. The corresponding curves are ruled by Equations (1)–(4), considering the material properties used in the parametric studies.

In the next figures, the horizontal axis is presented in a nondimensional way, while the vertical axis' units are referenced in the corresponding figures' legend.

It is very clear that different distributions lead to different properties evolutions and hence to different mechanical responses, thus demonstrating the ability to meet specific operating requirements.

Figure A1a,b illustrate the evolution of the Young's modulus through the thickness for the FGM jointly ruled by Equation (1) and by Equations (3) and (4), respectively.

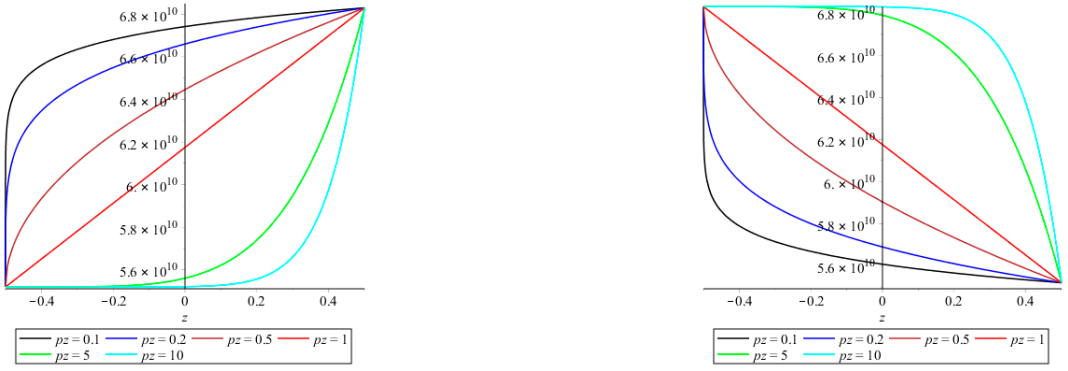

(**a**) (**b**)

Figure A1. Young's modulus evolution [Pa] of (**a**) FGM1-Z; (**b**) FGM2-Z.

Similarly for the density, and for the same two cases (Equations (3) and (4)), the profiles are depicted in Figure A2.

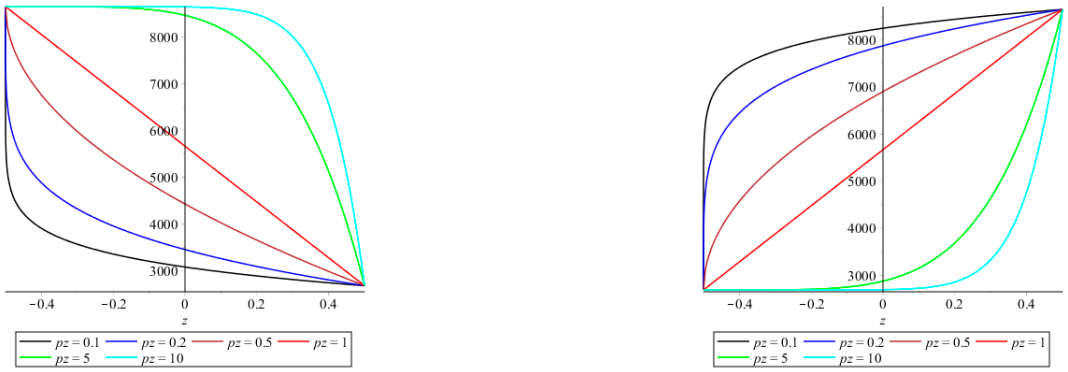

(**a**) (**b**)

Figure A2. Density evolution [kg.m^{-3}] of (**a**) FGM1-Z; (**b**) FGM2-Z.

The symmetrical mixture evolution along the beam length as jointly defined by Equations (2)–(4), is depicted for the Young's modulus distribution in Figure A3 and for the density in Figure A4.

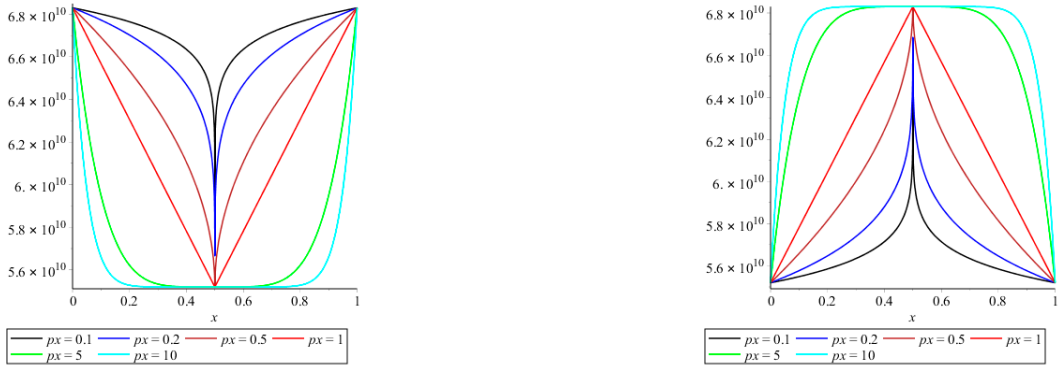

(**a**) (**b**)

Figure A3. Young's modulus evolution [Pa] of (**a**) FGM1-X; (**b**) FGM2-X.

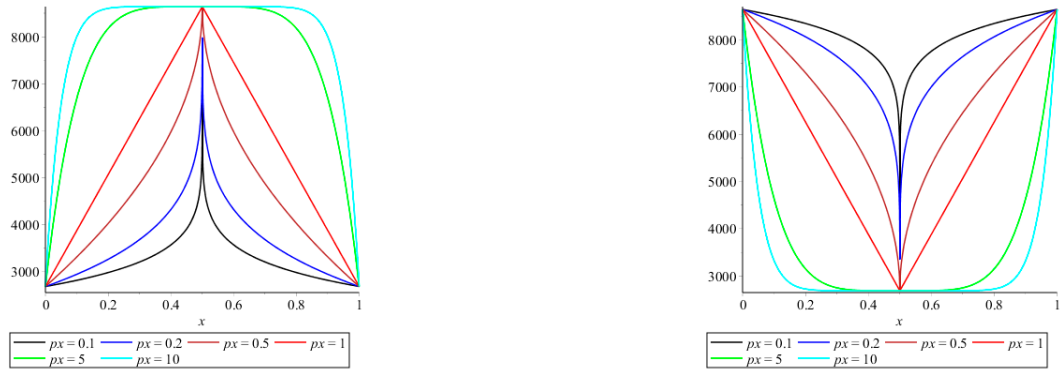

(**a**) (**b**)

Figure A4. Density evolution [kg.m^{-3}] of (**a**) FGM1-X; (**b**) FGM2-X.

References

1. Reddy, J. Nonlocal theories for bending, buckling and vibration of beams. *Int. J. Eng. Sci.* **2007**, *45*, 288–307. [CrossRef]
2. Eringen, A.C. Linear Theory of Non-Local Elasticity and Dispersion of plane waves. *Int. J. Eng. Sci.* **1972**, *10*, 425–435. [CrossRef]
3. Eringen, A.C. On differential equations of non local elasticity and solutions of screw dislocation and surface waves. *J. Appl. Phys.* **1983**, *54*, 4703–4710. [CrossRef]
4. Reddy, J.N.; Pang, S.D. Nonlocal continuum theories of beams for the analysis of carbon nanotubes. *J. Appl. Phys.* **2008**, *103*, 23511. [CrossRef]
5. Nejad, M.Z.; Hadi, A. Eringen's non-local elasticity theory for bending analysis of bi-directional functionally graded Euler–Bernoulli nano-beams. *Int. J. Eng. Sci.* **2016**, *106*, 1–9. [CrossRef]
6. Ghaffari, I.; Yaghoobi, M.P.; Ghannad, M. Complete mechanical behavior analysis of FG Nano Beam under non-uniform loading using non-local theory. *Mater. Res. Express* **2018**, *5*, 15016. [CrossRef]
7. Lu, L.; Guo, X.; Zhao, J. Size-dependent vibration analysis of nanobeams based on the nonlocal strain gradient theory. *Int. J. Eng. Sci.* **2017**, *116*, 12–24. [CrossRef]
8. Lu, L.; Guo, X.; Zhao, J. A unified nonlocal strain gradient model for nanobeams and the importance of higher order terms. *Int. J. Eng. Sci.* **2017**, *119*, 265–277. [CrossRef]
9. Danesh, H.; Javanbakht, M. Free vibration analysis of nonlocal nanobeams: A comparison of the one-dimensional nonlocal integral Timoshenko beam theory with the two-dimensional nonlocal integral elasticity theory. *Math. Mech. Solids* **2021**, *27*, 557–577. [CrossRef]
10. Koizumi, M. FGM activities in Japan. *Compos. Part B Eng.* **1997**, *28*, 1–4. [CrossRef]
11. Zhang, N.; Khan, T.; Guo, H.; Shi, S.; Zhong, W.; Zhang, W. Functionally Graded Materials: An Overview of Stability, Buckling, and Free Vibration Analysis. *Adv. Mater. Sci. Eng.* **2019**, *2019*, 1–18. [CrossRef]
12. Saleh, B.; Jiang, J.; Fathi, R.; Al-Hababi, T.; Xu, Q.; Wang, L.; Song, D.; Ma, A. 30 Years of functionally graded materials: An overview of manufacturing methods, Applications and Future Challenges. *Compos. Part B Eng.* **2020**, *201*, 108376. [CrossRef]
13. Rajak, D.K.; Pagar, D.D.; Kumar, R.; Pruncu, C.I. Recent progress of reinforcement materials: A comprehensive overview of composite materials. *J. Mater. Res. Technol.* **2019**, *8*, 6354–6374. [CrossRef]
14. El-Borgi, S.; Fernandes, R.; Reddy, J. Non-local free and forced vibrations of graded nanobeams resting on a non-linear elastic foundation. *Int. J. Non-Linear Mech.* **2015**, *77*, 348–363. [CrossRef]

15. Ebrahimi, F.; Barati, M.R. A nonlocal higher-order refined magneto-electro-viscoelastic beam model for dynamic analysis of smart nanostructures. *Int. J. Eng. Sci.* **2016**, *107*, 183–196. [CrossRef]
16. Hamed, M.A.; Eltaher, M.A.; Sadoun, A.M.; Almitani, K.H. Free vibration of symmetric and sigmoid functionally graded nanobeams. *Appl. Phys. A* **2016**, *122*, 829. [CrossRef]
17. Aria, A.I.; Friswell, M. A nonlocal finite element model for buckling and vibration of functionally graded nanobeams. *Compos. Part B Eng.* **2019**, *166*, 233–246. [CrossRef]
18. Rezaiee-Pajand, M.; Mokhtari, M. A novel meshless particle method for nonlocal analysis of two-directional functionally graded nanobeams. *J. Braz. Soc. Mech. Sci. Eng.* **2019**, *41*, 303. [CrossRef]
19. Katili, I.; Syahril, T.; Katili, A.M. Static and free vibration analysis of FGM beam based on unified and integrated of Timoshenko's theory. *Compos. Struct.* **2020**, *242*, 112130. [CrossRef]
20. Uzun, B.; Yaylı, M. Özgür Nonlocal vibration analysis of Ti-6Al-4V/ZrO2 functionally graded nanobeam on elastic matrix. *Arab. J. Geosci.* **2020**, *13*, 155. [CrossRef]
21. Akgöz, B.; Civalek, Ö. Bending analysis of FG microbeams resting on Winkler elastic foundation via strain gradient elasticity. *Compos. Struct.* **2015**, *134*, 294–301. [CrossRef]
22. Sobhy, M. A comprehensive study on FGM nanoplates embedded in an elastic medium. *Compos. Struct.* **2015**, *134*, 966–980. [CrossRef]
23. Rahaeifard, M. Size-dependent torsion of functionally graded bars. *Compos. Part B Eng.* **2015**, *82*, 205–211. [CrossRef]
24. Sobczak, J.J.; Drenchev, L. Metallic Functionally Graded Materials: A Specific Class of Advanced Composites. *J. Mater. Sci. Technol.* **2013**, *29*, 297–316. [CrossRef]
25. Chen, Y.; Liou, F. Additive Manufacturing of Metal Functionally Graded Materials: A Review. In Proceedings of the 29th Annual International Solid Freeform Fabrication Symposium—An Additive Manufacturing Conference, Austin, TX, USA, 13–15 August 2018; Volume 1, pp. 1215–1231.
26. Kumar, A.; Singh, R.; Chaudhary, R. Recent progress in production of metal matrix composites by stir casting process: An overview. *Mater. Today Proc.* **2020**, *21*, 1453–1457. [CrossRef]
27. Sudherson, D.P.S.; Sunil, J. Dry sliding wear behaviour of novel AA5083-cadmium alloy prepared by stir casting process. *Mater. Today Proc.* **2020**, *21*, 142–147. [CrossRef]
28. Mota, A.; Loja, M.; Singh, H.; Kalsi, S.B.S.; Barbosa, J.I. Image driven analysis of plates coated by cold spray coating process using a layerwise approach. *Compos. Struct.* **2021**, *261*, 113250. [CrossRef]
29. Mota, A.F.; Loja, M.A.R.; Barbosa, J.I.; Vinyas, M. Mechanical behavior of a sandwich plate with aluminum foam core, using an image-based layerwise model. *Mech. Adv. Mater. Struct.* **2021**, 1–30. [CrossRef]
30. Reddy, J.N. A General Nonlinear Third-Order Theory of Functionally Graded Plates. *Int. J. Aerosp. Light. Struct.* **2011**, *1*, 1–21. [CrossRef]
31. Carvalho, A.; Silva, T.A.N.; Loja, M.A.R.; Damásio, F.R. Assessing the influence of material and geometrical uncertainty on the mechanical behavior of FGM plates. *Mech. Adv. Mater. Struct.* **2017**, *24*, 417–426. [CrossRef]
32. Rosa, R.D.S.B.; Loja, M.A.R.; De Carvalho, A.C.J.V.N. Toward Variability Characterization and Statistic Models' Constitution for the Prediction of Exponentially Graded Plates' Static Response. *J. Compos. Sci.* **2018**, *2*, 59. [CrossRef]
33. Loja, M.; Barbosa, J.; Soares, C.M.M. A study on the modeling of sandwich functionally graded particulate composites. *Compos. Struct.* **2021**, *94*, 2209–2217. [CrossRef]
34. Bernardo, G.; Damásio, F.; Silva, T.; Loja, A. A study on the structural behaviour of FGM plates static and free vibrations analyses. *Compos. Struct.* **2016**, *136*, 124–138. [CrossRef]
35. Loja, M.; Barbosa, J. In-plane functionally graded plates: A study on the free vibration and dynamic instability behaviours. *Compos. Struct.* **2020**, *237*, 111905. [CrossRef]
36. Reddy, J.N. *Mechanics of Laminated Composite Plates and Shells: Theory and Analysis*; Taylor & Francis Inc.: Abingdon, UK, 1996; ISBN 9780849315923.
37. Nguyen, T.-K.; Sab, K.; Bonnet, G. First-order shear deformation plate models for functionally graded materials. *Compos. Struct.* **2008**, *83*, 25–36. [CrossRef]
38. Mota, A.F.; Loja, M.A.R.; Barbosa, J.I.; Rodrigues, J.A. Porous Functionally Graded Plates: An Assessment of the Influence of Shear Correction Factor on Static Behavior. *Math. Comput. Appl.* **2020**, *25*, 25. [CrossRef]
39. Loja, A.; Barbosa, J.; Scares, C. Buckling behaviour of laminated beam structures using a higher-order discrete model. *Compos. Struct.* **1997**, *38*, 119–131. [CrossRef]
40. Reddy, J.N. *Energy and Variational Methods in Applied Mechanics*; John Wiley & Sons Inc.: Hoboken, NJ, USA, 2002; ISBN 9780471896739.
41. Soares, C.M.; Correia, V.F.; Loja, M.R. Higher-order B-spline strip models for laminated composite structures with integrated sensors and actuators. *Compos. Struct.* **2001**, *54*, 267–274. [CrossRef]
42. Sina, S.; Navazi, H.; Haddadpour, H. An analytical method for free vibration analysis of functionally graded beams. *Mater. Des.* **2009**, *30*, 741–747. [CrossRef]
43. Simsek, M. Fundamental frequency analysis of functionally graded beams by using different higher-order beam theories. *Nucl. Eng. Des.* **2010**, *240*, 697–705. [CrossRef]